# Supplementary Material:
# Future projections and uncertainty assessment of precipitation extremes in the Korean peninsula from the CMIP6 ensemble

Yonggwan Shin[1], Yire Shin[1], Juyoung Hong[1], Maeong-Ki Kim[2], Young-Hwa Byun[3], Kyung-On Boo[3], Il-Ung Chung[4], Doo-Sun R. Park[5], and Jeong-Soo Park[1,*]

*1: Department of Statistics, Chonnam National University, Gwangju 500-757, Korea.*

*2: Department of Atmospheric Science, Kongju National University, Gongju, Korea.*

*3: Innovative Meteorological Research Department,*

*National Institute of Meteorological Sciences, Seogwipo, Korea.*

*4: Dept of Atmospheric and Environmental Sciences,*

*Gangneung-Wonju National University, Korea.*

*5: Dept. of Earth Sciences Education, Kyungpook National University, Daegu, Korea.*

**: Corresponding author, E-mail: jspark@jnu.ac.kr, Tel: +82-62-530-3445*

August 26, 2020

## 1 Data and simulation models

Figure S1 shows examples of time series plots of the observations, APHRODITE data [1], and the bias-corrected data, for the AMP1. The APHRODITE values of the AMP1 are smaller than the observations when comparing those data at near stations. Because of this difference, we applied a bias correction technique to the APHRODITE data, based on the observations of nearest neighbor stations.

Table S 1: The list of 21 CMIP6 (Coupled Model Intercomparison Project Phase 6) models analyzed in this study. The detaied information on each model are available at ESGF-node https://esgf-node.llnl.gov/projects/cmip6/.

| Model Name | Institution | Country | Resolution (Lon × Lat Level) |
|---|---|---|---|
| MIROC6 | JAMSTEC, AORI, NIES, R-CCS (MIROC) | Japan | 256×128 L81(T85) |
| BCC-CSM2-MR | Beijing Clim Center | China | 320×160 L46(T106) |
| CanESM5 | Canadian Centre Clim Model & Analysis, Enviro & Clim Change (CCCma) | Canada | 128×64 L49(T63) |
| MRI-ESM2.0 | Meteoro Research Institute (MRI) | Japan | 320×160 L80(TL159) |
| CESM2-WACCM | Nat Center for Atmos Res, Clim & Global Dynamics Lab (NCAR) | USA | 288×192 L70 |
| CESM2 | Nat Center for Atmos Res, Clim & Global Dynamics Lab (NCAR) | USA | 288×192 L32 |
| KACE1.0-GLOMAP | National Inst of Meteo Sci/Meteo Admin, Clim Res Div (NIMS-KMA) | Korea | 192×144 L85 |
| UKESM1-0-N96ORCA1 | MOHC & NERC, NIMS-KMA, NIWA | UK, Korea New Zealand | 192×144 L85 |
| MPI-ESM1.2-LR | Max Planck Inst for Meteo (MPI-M) | Germany | 192×96 L47(T63) |
| MPI-ESM1.2-HR | Max Planck Inst for Meteo (MPI-M) | Germany | 384×192 L95(T127) |
| INM-CM5-0 | Inst for Numerical Math, Russian Acad of Sci (INM) | Russia | 180×120 L73 |
| INM-CM4-8 | Inst for Numerical Math, Russian Acad of Sci (INM) | Russia | 180×120 L21 |
| IPSL-CM6A-LR | Institut Pierre Simon Laplace (IPSL) | France | 144×143 L79 |
| NorESM2-LM | NorESM Consortium of CICERO, MET-Norway, NERSC, NILU, UiB, UiO, UNI | Norway | 144×96 L32 |
| NorESM2-MM | NorESM Consortium of CICERO, MET-Norway, NERSC, NILU, UiB, UiO, UNI | Norway | 288×192 L32 |
| EC-Earth3-Veg | EC-Earth consortium, Swedish Meteo & Hydro Inst/SMHI, Sweden | EU | 512×256 L91(TL255) |
| EC Earth 3.3 | EC-Earth consortium, Swedish Meteo & Hydro Inst/SMHI, Sweden | EU | 512×256 L91(TL255) |
| ACCESS-CM2 | CSIRO, ARCCSS (Australian Res Council Centre of Excellence for Clim System Sci) | Australia | 192×144 L85 |
| ACCESS-ESM1-5 | Commonwealth Scientific & Industrial Res Organ (CSIRO) | Australia | 192×145 L38 |
| GFDL-ESM4 | National Oceanic & Atmos Admi, Geophy Fluid Dynamics Lab | USA | 360×180 L49 |
| FGOALS-g3 | Chinese Academy of Sciences (CAS) | China | 180×80 L26 |

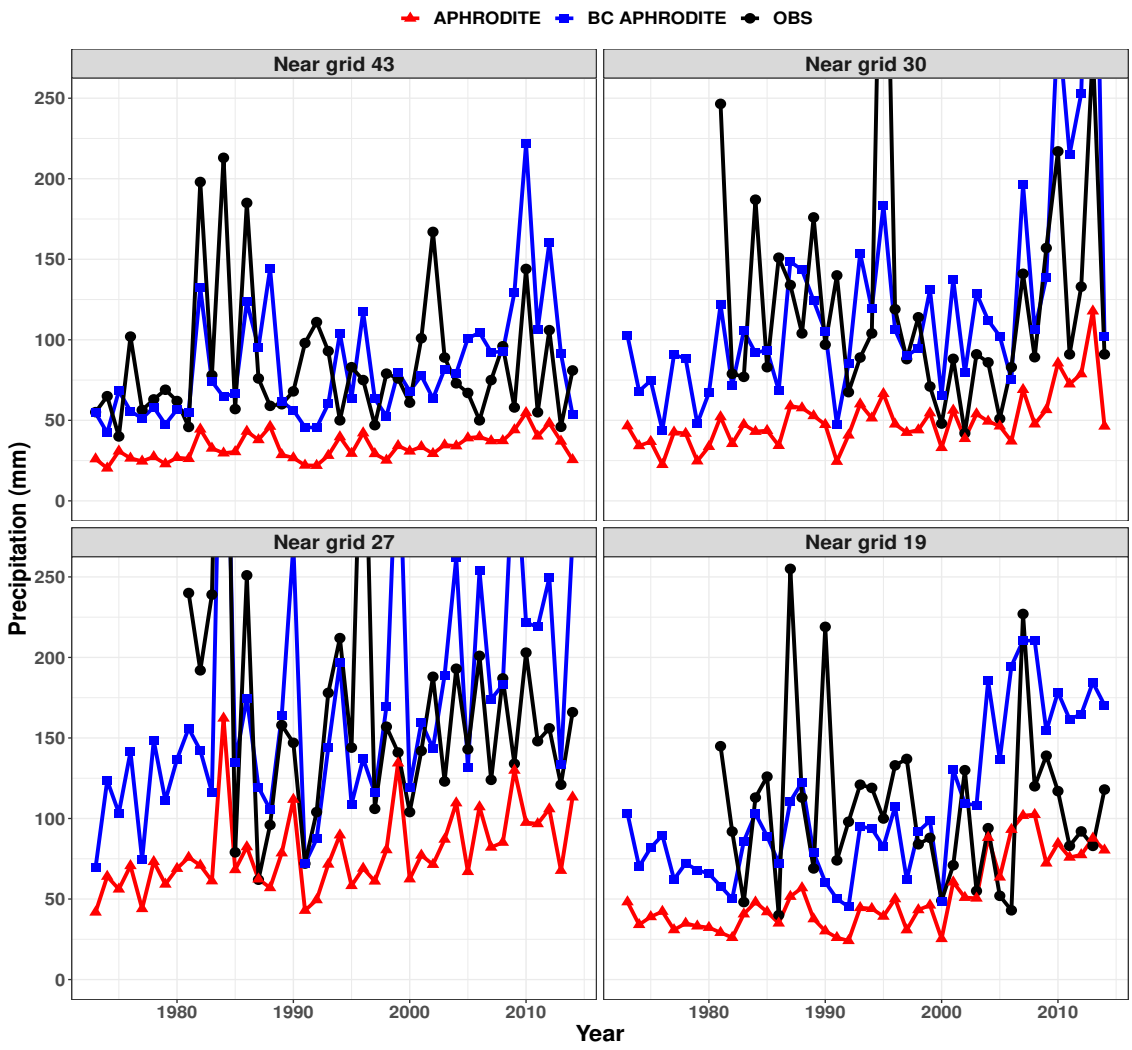


Figure S 1: Examples of time series plots of the observations, APHRODITE data, and the bias-corrected data.

# 2 Methods

## 2.1 Generalized extreme value distribution

Assuming the data approximately follow a GEV distribution, the parameters can be estimated by the maximum likelihood method[2, 3] or the method of L-moments estimation. The L-moments estimator is more efficient than the maximum likelihood estimator in small samples for typical shape parameter values [4]. The L-moments method is employed in this study

using the "lmom" package in R [5] because a relatively small number of samples are analyzed for each comparison period. Moreover, the formulae used to obtain the L-moments estimator are simple compared to that of obtaining the maximum likelihood estimator which needs an iterative optimization until convergence.

### 2.2 Bias correction: Multivariate generalization of quantile mapping

Some BC methods such as quantile mapping or delta change [6] make a perfect matching in the sense that the quantiles of the observations and the historical data are same. When the BC such as quantile mapping is used, most the model weights based on performance become equal because of a perfect matching, and consequently, the prediction is the simple average of bias-corrected model outputs. This is approximately true for the MBC [8] employed in this study because the MBC is a multivariate generalization of quantile mapping. Thus the historical data is not bias corrected. No-bias-corrected historical data are utilized to calculate the performance weight of a model.

Chen et al.[7] found that the joint BC of precipitation and air temperature led to a much better performance than univariate BC, in terms of hydrological modelling for all their studying basins located in various climates except for the coldest Canadian basin. Cannon [8] proposes a multivariate generalization of quantile mapping (QM). It is an iterative method which conceptually lays between univariate bias correction (BC) methods and the empirical copula-based correction (EC-BC) [9]. For a univariate BC, the quantile delta mapping (QDM) [10] is used, which preserves trends of model data

It approximately preserves the multivariate dependence of the driving climate model. Here, an image processing technique–the N-dimensional probability density function transform (N-pdft)–designed to transfer color information from one image to another is adapted. In each iteration, univariate QM is first applied separately to each variable. Then a linear multivariate BC is applied by re-scaling the multivariate anomalies based on Cholesky decomposition of the covariance matrix. The algorithm ends when both the corrected marginals and the dependence structure are sufficiently close to their observed counter parts. A variant is based on ranks rather than on the actual values [6]. It provides a multivariate quantile delta mapping, referred to as MBCn (multivariate bias correction with N-pdft) algorithm. It consists, in each iteration, of a random orthogonal rotation of multivariate input data, a univariate quantile delta mapping on the rotated fields and the inverse rotation. This algorithm approximately preserves trends of model data. We used 'MBC' package [11] in R for computation. The details are found in Cannon [8].

# 3 PI-weights

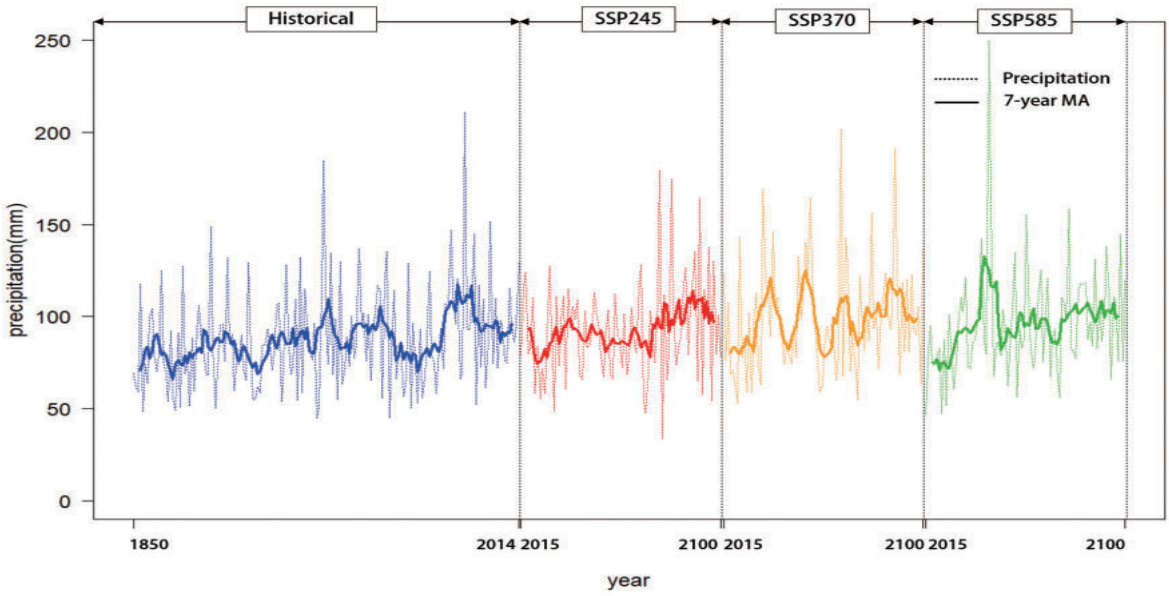


Figure S 2: Arrangement of data and 7-year moving averages composed of the historical data from 1850 to 2014 and the future data from 2015 to 2100 under SSP2, SSP3, and SSP5 scenarios for computing the Spearman correlation coefficient between models.

## 3.1 Computing independence weights

If a model has no close neighbors, then all $S_{ij}(i \neq j)$ are large, the denominator of the PI-weight is approximately one and has no effect. If two models $i$ and $j$ are identical, then $S_{ij} = 0$, the denominator equals two, so each model gets half the weight.

To calculate the model similarity $S_{ij}$, we follow a technique among several methods proposed by Sanderson et al.[12]. A method employed in this study is based on empirical orthogonal function (EOF) or principal component analysis. The following process is done for each grid: First, for each model, the historical data from 1850 to 2015 and the future simulation data from three scenarios are lined as one raw as in Figure S2. The bias correction is not applied to all data for this process. One can choose the historical data only as did by Brunner et al.[13], but we deploy all simulation data for a maximum use of available information. For each time series induced from each model, 7-year moving averages are obtained. Then, a correlation matrix $R$ among all $M$ models is constructed by applying the Spearman correlation coefficients

to those $M$ number of series of 7-year moving averages. That is, $R$ is the correlation matrix of $M$ models, with size $M \times M$.

A singular value decomposition (SVD) is performed on $R^{1/2}$ and truncated to $t$ modes to obtain the dominant modes of multivariate ensemble variability such that

$$R^{1/2} = U\lambda V^T, \tag{1}$$

where $U$ is an orthogonal matrix of model loadings (size $M$ by $t$) whose columns are the eigenvectors of the model correlation matrix $R$, $\lambda$ (size $t$ by $t$) are the eigenvalues of $R$, and $V$ (size $M$ by $t$) are the eigenvectors of $R$. The dimensions are sorted by decreasing eigenvalue, such that the basis set can be truncated to a smaller number of modes $t$ [12]. Note $t$ is often determined by selecting number of the eigenvalues greater than 1.

The model loadings $U$ now define a $t$-dimensional space (where $t$ is the truncation length of the SVD) in which intermodel and observation-model Euclidean distances may be defined. The intermodel distances can then be measured in a Euclidean sense in the loadings matrix, such that the distances $S_{ij}$ between two models $i$ and $j$ can be expressed as [12]

$$S_{ij} = \left\{ \sum_{l=1}^{t} [U(i,\, l) - U(j,\, l)]^2 \right\}^{1/2}. \tag{2}$$

$U(i,\, l)$ is interpreted as a correlation or a dependency of the model $i$ to the $l$-th principal component. Thus small $S_{ij}$ value means high dependency or similarity between models $i$ and $j$.

An example of the distances $S_{ij}$ between two models $i$ and $j$ calculated from Eq.(2) for some models is given in Table S2. Small value indicates high dependency or similarity between two models. In Table S2, the first 4 models show highest similarity whereas the last 4 models show lowest similarity.

## 3.2 Computing performance weights

To compute the performance of each model, $T$-year return levels are compared based on the GEVD fitting on the historical data and the observations. Let us denote $r_T^i$ and $r_T^0$ as $T$-year return level obtained from the historical data of $i$-th model and the observations, respectively. These values are normalized as follows to make it scale-free, for $i = 0, 1, \cdots, M$:

$$\tilde{r}_T^i = \frac{r_T^i - med_i}{R_i}, \tag{3}$$

Table S 2: The similarity distance metric $S_{ij}$ between model $i$ and model $j$ calculated from Eq.(2) for some models. Small value indicates high dependency or similarity between two models.

| | CanESM5 | ACCESS-CM2 | UKESM | KACE | NorESM2-LM | EC-Earth3 | FGOALS | INM-CM4 |
|---|---|---|---|---|---|---|---|---|
| CanESM5 | 0 | 0.40 | 0.40 | 0.37 | 0.46 | 0.52 | 0.69 | 0.73 |
| ACCESS-CM2 | 0.40 | 0 | 0.40 | 0.47 | 0.47 | 0.58 | 0.77 | 0.76 |
| KACE-1-0-G | 0.37 | 0.47 | 0.49 | 0 | 0.61 | 0.61 | 0.72 | 0.80 |
| UKESM | 0.40 | 0.40 | 0 | 0.49 | 0.50 | 0.59 | 0.73 | 0.75 |
| IPSL-CM6A-LR | 0.43 | 0.50 | 0.52 | 0.51 | 0.59 | 0.62 | 0.71 | 0.84 |
| ACCESS-ESM1-5 | 0.48 | 0.48 | 0.51 | 0.54 | 0.59 | 0.63 | 0.76 | 0.87 |
| NorESM2-LM | 0.46 | 0.47 | 0.50 | 0.61 | 0 | 0.56 | 0.82 | 0.81 |
| CESM2-WACCM | 0.46 | 0.55 | 0.55 | 0.44 | 0.68 | 0.63 | 0.81 | 0.82 |
| EC-Earth3-Veg | 0.48 | 0.53 | 0.54 | 0.51 | 0.59 | 0.65 | 0.78 | 0.76 |
| CESM2 | 0.54 | 0.55 | 0.53 | 0.54 | 0.63 | 0.64 | 0.83 | 0.81 |
| EC-Earth3 | 0.52 | 0.58 | 0.59 | 0.61 | 0.56 | 0 | 0.85 | 0.81 |
| NorESM2-MM | 0.53 | 0.58 | 0.59 | 0.59 | 0.74 | 0.75 | 0.84 | 0.76 |
| MPI-ESM1-2-LR | 0.50 | 0.64 | 0.62 | 0.51 | 0.68 | 0.65 | 0.79 | 0.84 |
| BCC-CSM2-MR | 0.59 | 0.56 | 0.58 | 0.58 | 0.69 | 0.73 | 0.82 | 0.91 |
| MPI-ESM1-2-HR | 0.64 | 0.63 | 0.65 | 0.68 | 0.63 | 0.69 | 0.82 | 0.87 |
| GFDL-ESM4 | 0.69 | 0.65 | 0.73 | 0.73 | 0.72 | 0.69 | 0.90 | 0.92 |
| MIROC6 | 0.70 | 0.70 | 0.68 | 0.68 | 0.78 | 0.75 | 0.89 | 0.96 |
| INM-CM5-0 | 0.62 | 0.73 | 0.69 | 0.70 | 0.74 | 0.74 | 0.94 | 0.87 |
| MRI-ESM2-0 | 0.66 | 0.75 | 0.73 | 0.74 | 0.79 | 0.82 | 0.89 | 0.88 |
| FGOALS-g3 | 0.69 | 0.77 | 0.73 | 0.72 | 0.82 | 0.85 | 0 | 0.99 |
| INM-CM4-8 | 0.73 | 0.76 | 0.75 | 0.80 | 0.81 | 0.81 | 0.99 | 0 |
| SUM | 10.89 | 11.70 | 11.78 | 11.82 | 13.08 | 13.51 | 16.35 | 16.76 |

where

$$R_i = \begin{cases} max_i - med_i & \text{if } r_T^i \geq med_i, \\ med_i - min_i & \text{if } r_T^i < med_i, \end{cases} \tag{4}$$

and $max_i$, $min_i$, and $med_i$ are the maximum, the minimum, and the median of $i$-th model data. Other ways of standardizations are also possible.

The distance for performance measure is obtained by

$$D_i^2 = \sum_T (\tilde{r}_T^i - \tilde{r}_T^0)^2. \tag{5}$$

We set $T = 2$, 5, 10, 20, 30, 50, and 100. Note that $D_i$ does not depend on the shape parameter $\sigma_D$, and so obtained $D_i$s are fixed for the next computation.

### 3.3 Computing the p-value in selecting $\sigma_D$

The p-values in the manuscript are computed by a Monte-Carlo simulation in which random numbers of weights are generated from the Dirichlet distribution [14]. When the parameters are all equal to 1, the Dirichlet distribution is same as the multivariate uniform distribution with values between 0 and 1, which represents the null hypothesis. We used 'MCMCpack' package [15] in R to generate the random weights satisfying $H_0$.

The detailed steps of computing the p-value for given $\sigma_D$ and $\chi_0^2(\sigma_D)$ are:

**Step 1:** Generate random weights $P_i^{(k)}$ from the Dirichlet distribution with all parameters equal to 1 (under $H_0$), for $i = 1, \cdots, M$

**Step 2:** Compute $\chi^2 = \sum_{i=1}^{M} \frac{(\frac{1}{M} - P_i^{(k)})^2}{1/M}$, and denote it $\chi_{(k)}^2$

**Step 3:** Iterate the above two Steps K (=1,000 for example) times

**Step 4:** Calculate $p - value(\sigma_D) = \sum_{k=1}^{K} \frac{I\,[\chi_{(k)}^2 > \chi_0^2(\sigma_D)]}{K}$,

where $I[A]$ denotes the identity function which takes 1 or 0 according that the condition $A$ is satisfied or not. Note that $P_i^{(k)}$s generated in Step 1 do not depend on $\sigma_D$.

## 4 Result: Future projection of extreme rainfall

The relative change of 20-year return level in the period P1 relative to the reference period P0 is defined as:

$$\delta R_{20}(P1) = \frac{R_{20}(P1) - R_{20}(P0)}{R_{20}(P0)} \times 100, \tag{6}$$

where $R_{20}(P)$ is the 20-year return level in the period P.

### 4.1 Return period and exceedance probability

We have experienced some technical flows in computing the waiting time or the return periods corresponding to a return value. For example, the resulting return period sometimes turns out to be greater than 500 years even though it is expected to correspond to 50 years. It may be due to the cumulation of truncation or rounding errors in computer, related to inverting the quantile function of the GEVD. A trouble caused by this flow does not vanish even applied to unequally weighted regional frequency analysis (RFA). In this study, we thus adopted the trimmed mean [3] in RFA in which unfairly very high estimates of return periods are deleted

Table S 3: Statistics of 20-year and 50-year return levels of the annual maximum daily precipitation (unit: mm) averaged over 46 grids in the Korean peninsula for the observations (OBS) and the future periods; P1 (2021-2050), P2 (2046-2075), and P3 (2071-2100) under the SSP2, SSP3, and SSP5 scenarios.

| | | | SSP2-4.5 | | | SSP3-7.0 | | | SSP5-8.5 | | |
|---|---|---|---|---|---|---|---|---|---|---|---|
| | Statistic | OBS | P1 | P2 | P3 | P1 | P2 | P3 | P1 | P2 | P3 |
| 20-year | Mean | 216 | 230 | 240 | 249 | 226 | 244 | 263 | 232 | 256 | 285 |
| | Q1 | 185 | 203 | 206 | 224 | 195 | 217 | 236 | 194 | 224 | 259 |
| | Median | 230 | 243 | 251 | 254 | 238 | 255 | 281 | 249 | 269 | 295 |
| | Q3 | 250 | 260 | 273 | 285 | 259 | 276 | 300 | 271 | 301 | 322 |
| 50-year | Mean | 267 | 279 | 293 | 305 | 273 | 297 | 322 | 280 | 313 | 351 |
| | Q1 | 231 | 254 | 257 | 280 | 235 | 273 | 296 | 235 | 276 | 319 |
| | Median | 276 | 285 | 306 | 319 | 285 | 308 | 331 | 291 | 327 | 366 |
| | Q3 | 303 | 309 | 332 | 345 | 306 | 334 | 363 | 319 | 357 | 392 |

in computing the weighted average. The defects of return periods are described in Serinaldi [16].

The spatially averaged estimates of exceedance probability are presented in Figure S6 and in Table S6.

# 5 Results: Quantifying uncertainty

From the analysis of variance, Figure S7 shows the interaction plots of 20-year return levels from 21 CMIP6 for 3 SSP scenarios over 3 periods. In this figure, the return levels of some models such as CESM2-WACOM, ACCESS-ESM1-5, NorESM2-MM, MiCRO6, MRI-ESM2-0, and GFDL-ESM4 decrease from the SSP2 to the SSP3, contrary to the expectation. Moreover, the return values of some models such as MPI-ESM1-2-HR, MPI-ESM1-2-LR, and NorESM2-LM decrease from the SSP3 to the SSP5. Figure S8 shows the interaction plots between 21 CMIP6 and the latitude in which the latitude changes from $33^o$ to $43^o$, for 20-year return levels (unit: mm).

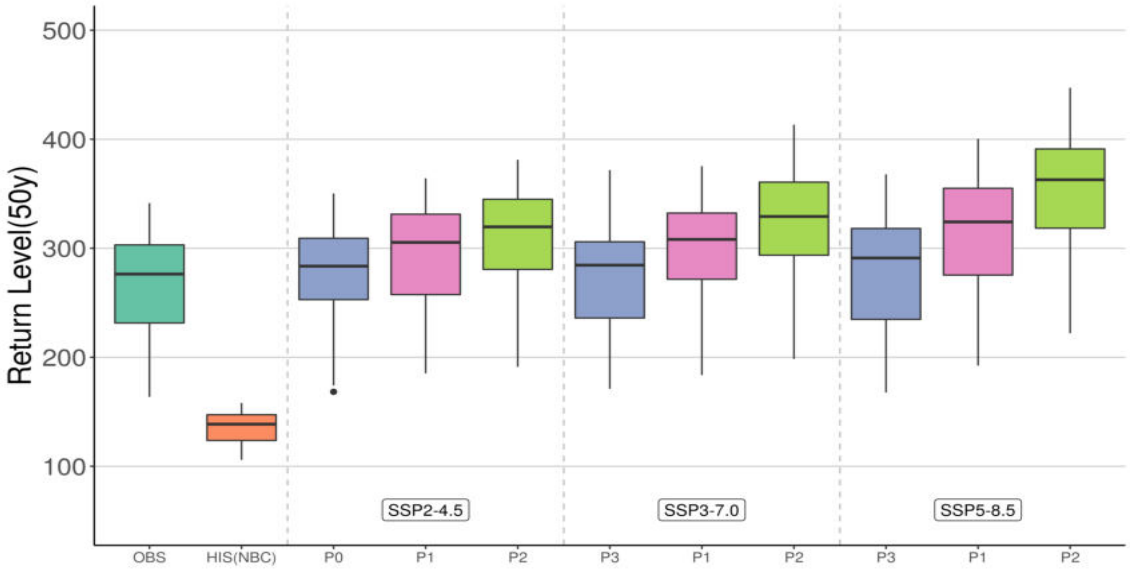


Figure S 3: Schematic box-plots of 50-year return levels of the annual maximum daily precipitation (unit: mm) averaged over 46 grids in the Korean peninsula for the future periods P1 (2021-2050), P2 (2046-2075), and p3 (2071-2100) under the SSP2, SSP3, and SSP5 scenarios. OBS and HIST(NBC) stand for the observations and the historical data without bias correction. The box-plot for p0 represents the bias-corrected historical data.

# References


[1] Yatagai A, Kamiguchi K, Arakawa O, Hamada A, Yasutomi N, Kitoh A (2012) APHRODITE: Constructing a long–term daily griddied precipitation dataset for Asia based on a dense network of rain gauges. Bull Amer Meteorol Soc 93:1401–1415.

[2] Coles S (2001) *An Introduction to Statistical Modelling of Extreme Values.* Springer, New York, pp 224.

[3] Wilks D (2011) *Statistical Methods in the Atmospheric Sciences,* 3rd Ed., Academic Press, New York.

[4] Hosking JRM, Wallis JR (1997) *Regional frequency analysis: An approach based on L-moments*, Cambridge University Press, Cambridge, 244pp.

[5] Hosking JRM (2019) L-Moments. R package, version 2.8. https://CRAN.R-project.org/package=lmom.

[6] Maraun D, Widmann M (2018) *Statistical downscaling and bias correction for climate research.* Cambridge Univ Press.

Table S 4: Relative change (unit: %) in 20-year and 50-year return levels of the annual maximum daily precipitation averaged over the Korean peninsula relative to 1973–2014.

| | | SSP2-4.5 | | | SSP3-7.0 | | | SSP5-8.5 | | |
|---|---|---|---|---|---|---|---|---|---|---|
| | | p1 | p2 | p3 | p1 | p2 | p3 | p1 | p2 | p3 |
| 20-year | Mean | 7.1 | 11.7 | 16.4 | 4.9 | 13.3 | 22.5 | 7.2 | 19.2 | 33.4 |
| | Q1 | 3.2 | 8.2 | 12.0 | 4.2 | 10.4 | 18.7 | 4.7 | 11.6 | 21.3 |
| | Median | 6.9 | 10.7 | 16.4 | 5.1 | 13.0 | 22.9 | 7.3 | 21.4 | 37.6 |
| | Q3 | 10.7 | 15.4 | 21.6 | 6.3 | 16.6 | 26.9 | 10.4 | 24.4 | 42.0 |
| 50-year | Mean | 6.3 | 11.3 | 16.4 | 3.4 | 12.5 | 22.4 | 5.9 | 19.1 | 34.0 |
| | Q1 | 1.2 | 7.5 | 11.8 | 1.3 | 9.8 | 17.3 | 1.8 | 9.8 | 19.6 |
| | Median | 5.2 | 10.6 | 16.5 | 3.9 | 12.0 | 22.8 | 5.7 | 20.6 | 35.4 |
| | Q3 | 10.3 | 15.5 | 22.6 | 5.6 | 15.8 | 26.1 | 10.3 | 25.0 | 45.8 |

Table S 5: Statistics of 20-year and 50-year return periods (unit: year) of the annual maximum daily precipitation averaged over 46 grids in the Korean peninsula for the future periods P1 (2021-2050), P2 (2046-2075), and p3 (2071-2100) under the SSP2, SSP3, and SSP5 scenarios.

| | | SSP2-4.5 | | | SSP3-7.0 | | | SSP5-8.5 | | |
|---|---|---|---|---|---|---|---|---|---|---|
| | | P1 | P2 | P2 | P1 | P2 | P3 | P1 | P2 | P3 |
| 20-year | Mean | 18.0 | 13.7 | 12.0 | 18.4 | 13.7 | 10.3 | 17.2 | 11.5 | 7.8 |
| | Q1 | 16.4 | 12.5 | 10.9 | 14.7 | 11.6 | 9.5 | 14.2 | 10.4 | 6.8 |
| | Median | 17.6 | 13.4 | 11.9 | 18.6 | 13.8 | 10.1 | 17.0 | 12.1 | 7.6 |
| | Q3 | 20.0 | 15.2 | 13.0 | 21.0 | 15.6 | 11.4 | 20.6 | 13.5 | 9.2 |
| 50-year | Mean | 42.2 | 37.2 | 30.8 | 47.0 | 33.2 | 25.6 | 39.8 | 29.6 | 19.1 |
| | Q1 | 35.9 | 33.7 | 26.6 | 41.8 | 28.4 | 22.7 | 36.7 | 26.4 | 16.0 |
| | Median | 42.0 | 35.5 | 30.2 | 48.9 | 33.6 | 24.9 | 41.8 | 29.9 | 18.6 |
| | Q3 | 47.6 | 41.2 | 33.9 | 52.6 | 37.0 | 28.6 | 44.7 | 34.9 | 22.1 |


[7] Chen J, Li C, Brissette FP, Chen H, Wang M, Essou GRC (2018) Impacts of correcting the inter-variable correlation of climate model ouputs on hydrological modeling. J Hydrol 560:326–341.

[8] Cannon AJ (2018) Multivariate quantile mapping bias correction: an N-dimensional probability density function transform for climate model simulations of multiple variables. Clim Dyn 50:31–49.

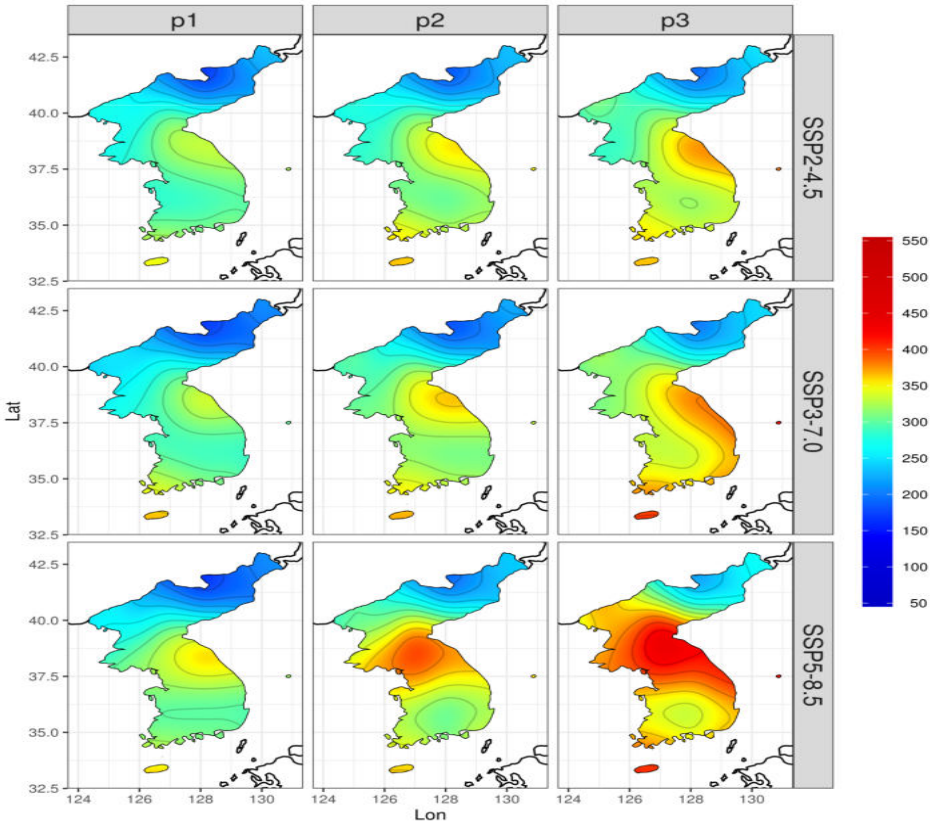


Figure S 4: Isopluvial maps of 50-year return levels of the annual maximum daily precipitation for 46 grids over the Korean peninsula for the future periods P1 (2021-2050), P2 (2046-2075), and P3 (2071-2100) under the SSP2, SSP3, and SSP5 scenarios.


[9] Vrac M, Friederichs P (2015) Multivariate-intervariable, spatial, and temporal-bias correction. J Clim 28:218–237.

[10] Cannon AJ, Sobie SR, Murdock TQ (2015) Bias correction of GCM precipitation by quantile mapping: How well do methods preserve changes in quantiles and extremes? J Climate 28:6938–6959.

[11] Cannon AJ (2018) Package 'MBC' in R, version 0.10-4. https://cran.r-project.org/web/packages/MBC/MBC.pdf

[12] Sanderson BM, Knutti R, Caldwell P (2015a) Addressing interdependency in a multimodel ensemble by interpolation of model properties. J Clim 28:5150-70.

[13] Brunner L, Pendergrass AG, Lehner F, Merrifield AL, Lorenz R, Knutti R (2020) Reduced global warming from CMIP6 projections when weighting models by performance and independence. Earth System Dynamics Discussion. Preprint Doi:10.5194/esd-2020-23

Table S 6: spatially averaged the exceedance probability for the annual maximum daily precipitation (AMP1) from $50mm$ to $300mm$, obtained from the observations (OBS) and the CMIP6 models under the three scenarios for three future periods.

| | AMP1 | OBS | SSP2-4.5 | SSP3-7.0 | SSP5-8.5 |
|---|---|---|---|---|---|
| Period 1 | 50 mm | 0.989 | 0.989 | 0.990 | 0.991 |
| | 100 mm | 0.531 | 0.704 | 0.687 | 0.705 |
| | 150 mm | 0.149 | 0.240 | 0.222 | 0.238 |
| | 200 mm | 0.048 | 0.069 | 0.069 | 0.063 |
| | 250 mm | 0.019 | 0.024 | 0.021 | 0.022 |
| | 300 mm | 0.008 | 0.009 | 0.008 | 0.010 |
| Period 2 | 50 mm | 0.989 | 0.988 | 0.990 | 0.992 |
| | 100 mm | 0.531 | 0.712 | 0.748 | 0.789 |
| | 150 mm | 0.149 | 0.238 | 0.300 | 0.312 |
| | 200 mm | 0.048 | 0.080 | 0.097 | 0.110 |
| | 250 mm | 0.019 | 0.027 | 0.034 | 0.038 |
| | 300 mm | 0.008 | 0.013 | 0.018 | 0.019 |
| Period 3 | 50 mm | 0.989 | 0.990 | 0.992 | 0.993 |
| | 100 mm | 0.531 | 0.755 | 0.793 | 0.822 |
| | 150 mm | 0.149 | 0.262 | 0.343 | 0.384 |
| | 200 mm | 0.048 | 0.086 | 0.127 | 0.161 |
| | 250 mm | 0.019 | 0.032 | 0.048 | 0.062 |
| | 300 mm | 0.008 | 0.015 | 0.019 | 0.033 |


[14] Everitt BS, Skrondal A (2010) *The Cambridge Dictionary of Statistics*, Cambridge University Press.

[15] Martin AD, Quinn KM, Park JH (2011) MCMCpack: Markov Chain Monte Carlo in R. Journal of Statistical Software 42(9)

[16] Serinaldi F (2015) Dismissing return periods! Stoch Environ Res Risk Assess 29:1179–1189. https://doi.org/10.1007/s00477-014-0916-1

Table S 7: The expected waiting time (unit: year) until reoccurrence or the return period of specific the annual maximum daily precipitation (AMP1) values from $50mm$ to $300mm$, obtained from the observations (OBS) and the CMIP6 models under the 3 scenarios for 3 future periods.

| | | SSP2-4.5 | | | SSP3-7.0 | | | SSP5-8.5 | | |
|---|---|---|---|---|---|---|---|---|---|---|
| AMP1 | OBS | P1 | P2 | P3 | P1 | P2 | P3 | P1 | P2 | P3 |
| 50 mm | 1.0 | 1.0 | 1.0 | 1.0 | 1.0 | 1.0 | 1.0 | 1.0 | 1.0 | 1.0 |
| 100 mm | 1.9 | 1.4 | 1.4 | 1.3 | 1.5 | 1.3 | 1.3 | 1.4 | 1.3 | 1.2 |
| 150 mm | 6.7 | 4.2 | 4.2 | 3.8 | 4.5 | 3.3 | 2.9 | 4.2 | 3.2 | 2.6 |
| 200 mm | 20.8 | 14.5 | 12.5 | 11.6 | 14.6 | 10.4 | 7.8 | 15.9 | 9.1 | 6.2 |
| 250 mm | 52.6 | 41.2 | 37.3 | 31.6 | 47.8 | 29.5 | 20.8 | 46.1 | 26.4 | 16.1 |
| 300 mm | 118.8 | 107.0 | 79.4 | 65.0 | 123.5 | 57.4 | 52.1 | 99.4 | 53.2 | 30.5 |

Table S 8: The expected frequency of reoccurring years during 30 years for specific the annual maximum daily precipitation (AMP1) values from $50mm$ to $300mm$, obtained from the observations (OBS) and the CMIP6 models under the 3 scenarios for 3 future periods

| | | SSP2-4.5 | | | SSP3-7.0 | | | SSP5-8.5 | | |
|---|---|---|---|---|---|---|---|---|---|---|
| AMP1 | OBS | P1 | P2 | P3 | P1 | P2 | P3 | P1 | P2 | P3 |
| 50 mm | 29.7 | 29.7 | 29.6 | 29.7 | 29.7 | 29.7 | 29.8 | 29.7 | 29.8 | 29.8 |
| 100 mm | 15.9 | 21.1 | 21.4 | 22.6 | 20.6 | 22.4 | 23.8 | 21.1 | 23.7 | 24.7 |
| 150 mm | 4.5 | 7.2 | 7.1 | 7.9 | 6.7 | 9.0 | 10.3 | 7.1 | 9.4 | 11.5 |
| 200 mm | 1.4 | 2.1 | 2.4 | 2.6 | 2.1 | 2.9 | 3.8 | 1.9 | 3.3 | 4.8 |
| 250 mm | 0.6 | 0.7 | 0.8 | 1.0 | 0.6 | 1.0 | 1.4 | 0.7 | 1.1 | 1.9 |
| 300 mm | 0.2 | 0.3 | 0.4 | 0.4 | 0.2 | 0.5 | 0.6 | 0.3 | 0.6 | 1.0 |

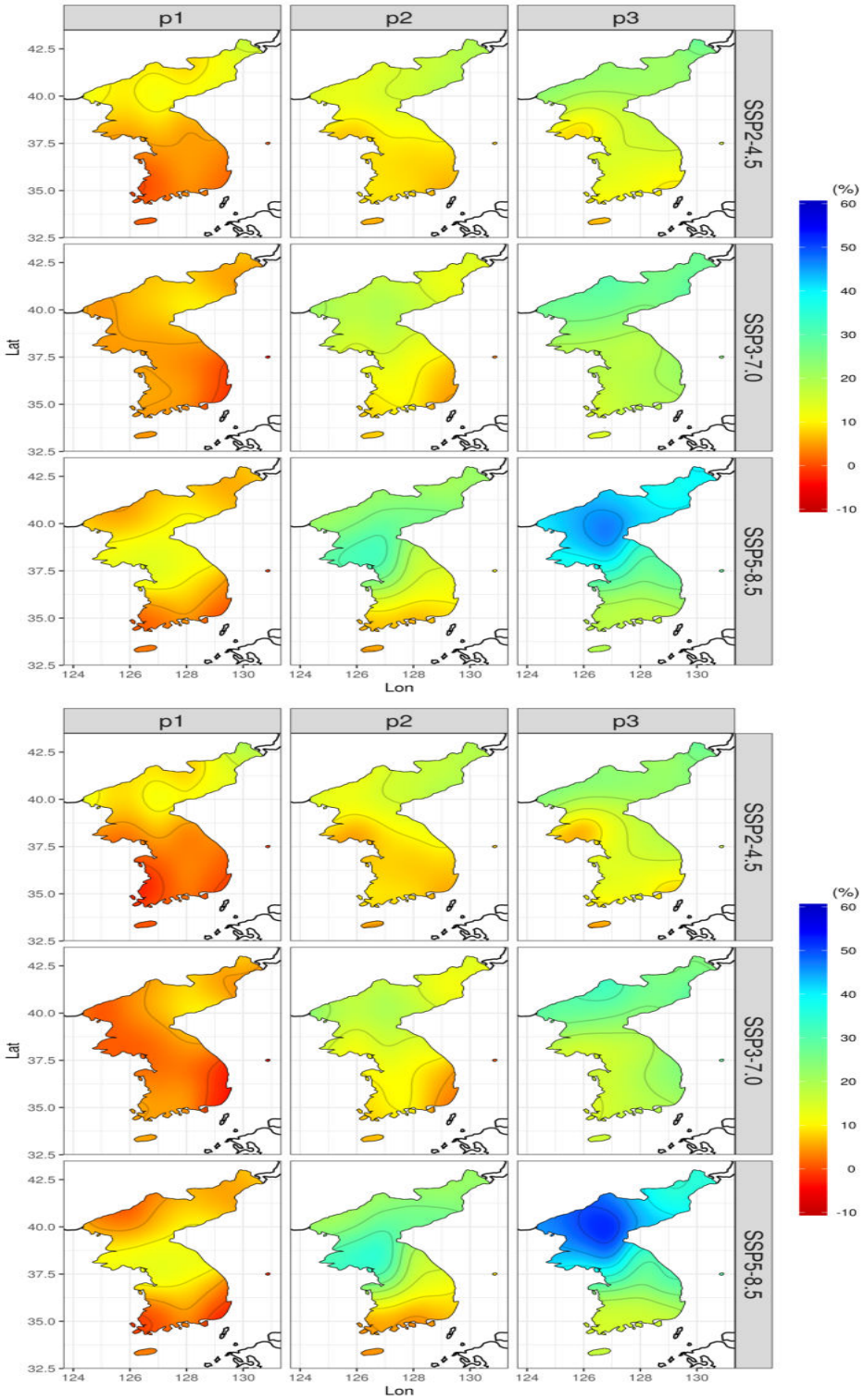


Figure S 5: Isopluvial maps of for the relative changes (unit: %) of 20-year and 50 return levels relative to 1973–2014 for the annual maximum daily precipitation for 46 grids over the Korean peninsula for the future periods P1 (2021-2050), P2 (2046-2075), and p3 (2071-2100) under the SSP2, SSP3, and SSP5 scenarios.

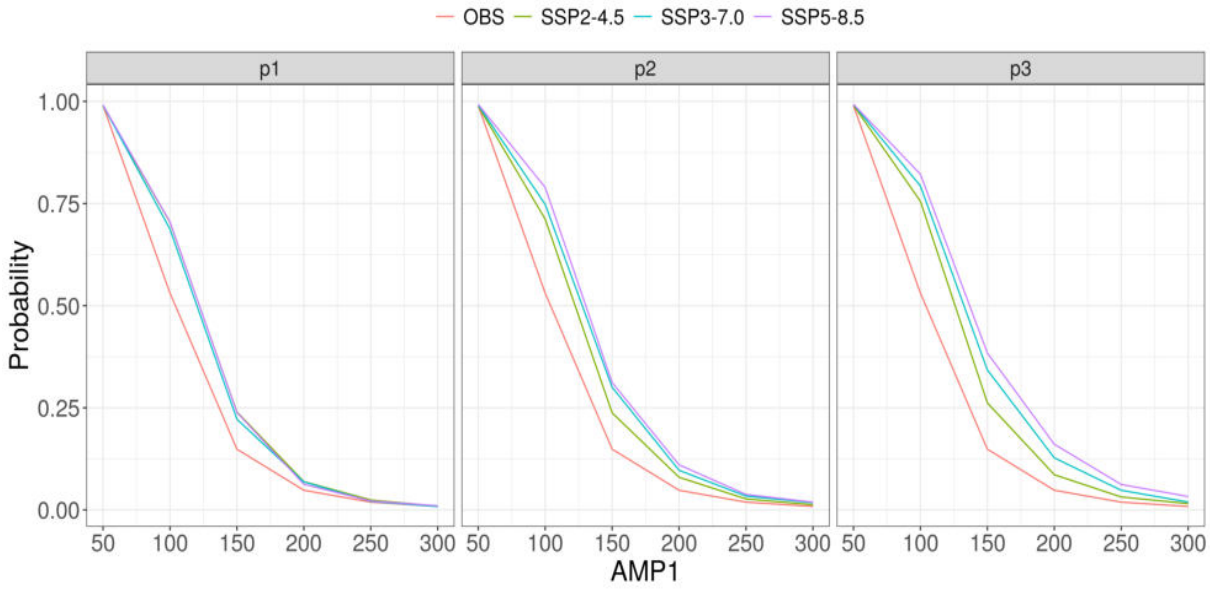


Figure S 6: The exceedance probability plots for the annual maximum daily precipitation (AMP1) from $50mm$ to $300mm$, obtained from the observations (OBS) and the CMIP6 models under the three scenarios for three future periods.

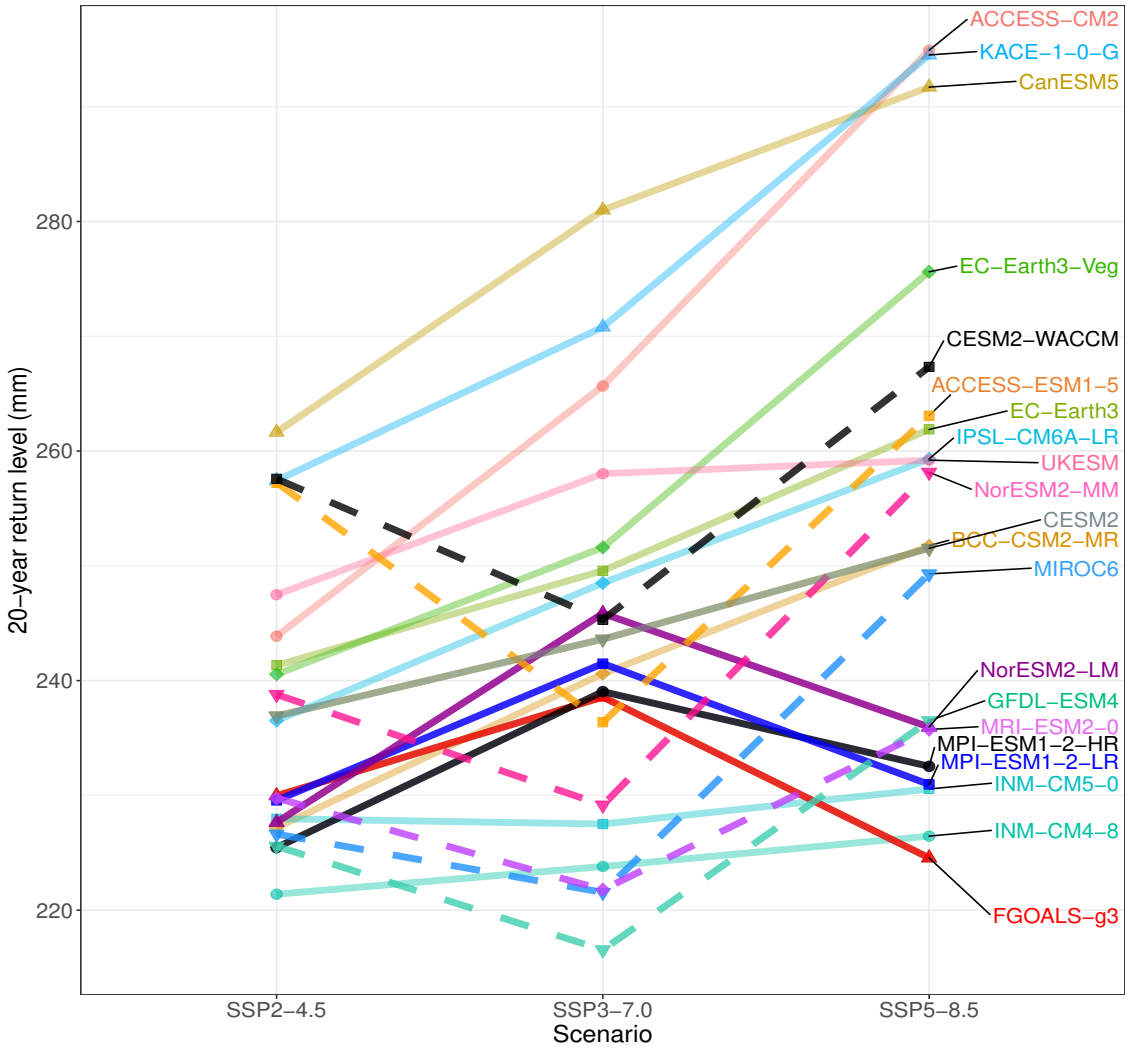


Figure S 7: Interaction plots of 20-year return levels from 21 CMIP6 for 3 SSP scenarios, averaged over 3 periods and 46 grids.

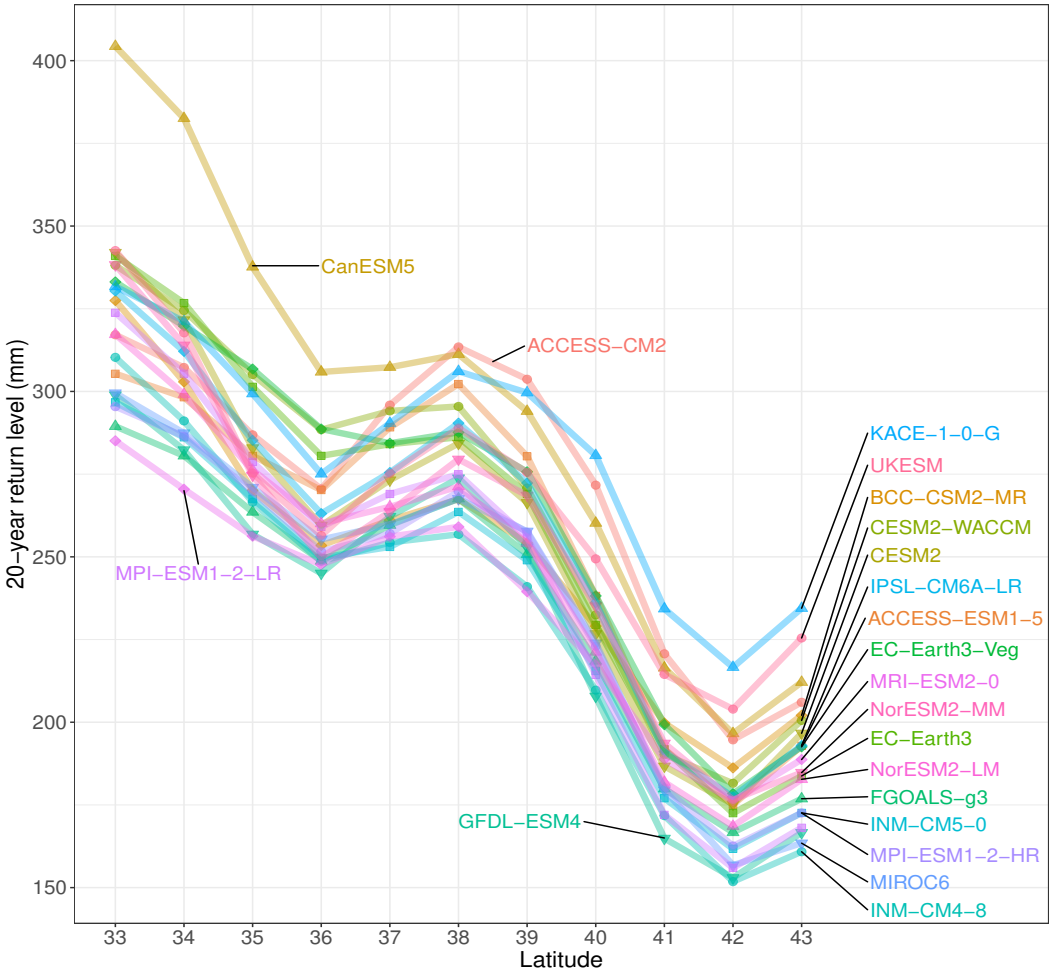


Figure S 8: Interaction plots between 21 CMIP6 and the latitude in which the latitude changes from $33^o$ to $43^o$, for 20-year return levels (unit: mm).